ADVANCED FUNCTIONAL MATERIALS
www.afm-journal.de

Check for updates

Charge Carrier Mobility and Series Resistance Extraction in 2D Field-Effect Transistors: Toward the Universal Technique

*Yu-Chieh Chien, Xuewei Feng, Li Chen, Kai-Chun Chang, Wee Chong Tan, Sifan Li, Li Huang, and Kah-Wee Ang**

2D semiconductor field-effect transistors (2D FETs) have emerged as a promising candidate for beyond-silicon electronics applications. However, its device performance has often been limited by the metal-2D semiconductor contact, and the non-negligible contact resistance (R_{SD}) not only deteriorates the on-state current but also hinders the direct characterization of the intrinsic properties of 2D semiconductors (e.g., intrinsic charge carrier mobility, μ_{int}). Therefore, a proper extraction technique that can independently characterize the metal-2D semiconductor contact behavior and the intrinsic properties of a 2D semiconducting layer is highly desired. In this study, a universal yet simple method is developed to accurately extract the critical parameters in 2D FETs, including characteristic temperature (T_o), threshold voltage (V_T), R_{SD}, and μ_{int}. The practicability of this method is extensively explored by characterizing the temperature-dependent carrier transport behavior and the strain-induced band structure modification in 2D semiconductors. Technology computer aided design simulation is subsequently employed to verify the precision of R_{SD} extraction. Furthermore, the universality of the proposed method is validated by successfully implementing the extraction to various 2D semiconductors, including black phosphorus, indium selenide, molybdenum disulfide, rhenium disulfide, and tungsten disulfide with top- and bottom-gated configurations.

1. Introduction

Contact resistance (R_{SD}) is an essential parameter in modern electronic devices that predominantly governs the electrical performance. Several semiconducting materials have been deemed as promising candidates for future technology nodes due to their attractive electronic and physical properties. For instance, 2D semiconductors serve as a performance booster for high-density device integration in silicon back-end-of-line (BEOL) due to their atomically thin nature that is ideally immune to the surface scattering effect.[1–3] The potential to realize wafer-scale integration of 2D semiconductors in field-effect transistors (FETs) has been recently demonstrated by several research groups.[4–7] Although 2D semiconductors manifest several fascinating properties, the electrical performance has been experimentally proven less competitive than those predicted from ab initio calculations.[8–10] One of the main reasons arising from the considerable effect of R_{SD}, which hinders the carrier transport through the semiconducting channel and deteriorates the on-state drain current (I_D). Additionally, the non-negligible R_{SD} effect increases the difficulty of probing the intrinsic properties in 2D semiconductors, such as the intrinsic charge carrier (μ_{int}), which hampers the understanding of the underlying device physics of 2D FETs. Accurate characterization of 2D FETs is, however, non-trivial to further improve its electrical performance and to realize the practical applications based on 2D materials.

To unveil the fundamental device parameters in 2D FETs (i.e., μ_{int}), one has to explicitly account for the R_{SD} effects in the extraction procedure. The transfer length method (TLM) is an intuitive approach that can be utilized to separately determine the R_{SD} and μ_{int} from the total resistance (R_o) versus channel length (L_{ch}) plot. Linear regression is subsequently performed where the R_{SD} and μ_{int} can be extracted by the y-intercept and slope, respectively.[11] Although TLM has been widely adopted in characterizing FETs, this method explicitly assumes an identical contact behavior and a uniform film quality of the semiconducting layer across the test structures, which could sometimes be challenging for 2D FETs. A large set of devices with various L_{ch} conditions is typically required to produce reliable extraction results. Indeed, recent studies have suggested that the erroneous extraction could be easily introduced by TLM, and additional steps are required to preserve its accuracy.[12–14]

Y.-C. Chien, X. Feng, L. Chen, W. C. Tan, S. Li, L. Huang, K.-W. Ang
Department of Electrical and Computer Engineering
National University of Singapore
4 Engineering Drive 3, Singapore 117583, Singapore
E-mail: eleakw@nus.edu.sg

K.-C. Chang
Department of Physics
National Sun Yat-Sen University
70 Lien-hai Road, Kaohsiung 80424, Taiwan

K.-W. Ang
Institute of Materials Research and Engineering
A*STAR
2 Fusionopolis Way, Singapore 138634, Singapore

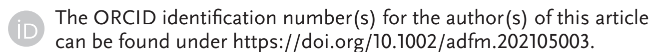
The ORCID identification number(s) for the author(s) of this article can be found under https://doi.org/10.1002/adfm.202105003.

© 2021 The Authors. Advanced Functional Materials published by Wiley-VCH GmbH. This is an open access article under the terms of the Creative Commons Attribution-NonCommercial-NoDerivs License, which permits use and distribution in any medium, provided the original work is properly cited, the use is non-commercial and no modifications or adaptations are made.

DOI: 10.1002/adfm.202105003

 © 2021 The Authors. Advanced Functional Materials published by Wiley-VCH GmbH

To facilitate the extraction, one may prefer to extract R_{SD} and μ_{int} from a standalone device that can effectively avoid the extraction error while simultaneously study the device-to-device variation.

Several techniques, including resistance extrapolation, asymptotical behavior, *Y*-function, *H*-function, and *F*-function methods, have been developed to characterize the essential parameters from a standalone bulk semiconductor FET, but less effort has been made in 2D semiconductors.[15–22] In addition, the applicability of these methods to 2D FETs has not been systematically verified.[18] For instance, the analytical expression of the intrinsic charge carrier mobility has been explicitly modeled as $\mu_{int} = \frac{\mu_{LF}}{1+\theta_o(V_G - V_T)}$ in the *Y*-function method, where μL_F is the low-field mobility and θ_o is the first-order mobility attenuation factor. This μ_{int} expression is, however, valid only when i) defect-affected transport behavior is fully negligible, and ii) phonon/surface scattering events are the only dominating factors that determine the carrier conduction through the semiconducting channel. On the other hand, a power-law μ_{int} expression, $\mu_{int} = \mu_o(V_G - V_T)^\gamma$ has been employed in the integration-based techniques, namely the *H*- and *F*-function methods.[19–22] This power-law expression is first derived for hydrogenated-amorphous silicon thin-film transistors (a-Si:H TFTs), in which the mobility enhancement factor, γ, can be correlated to the tail-distributed trap states in the forbidden band.[23] It has also been argued that the carrier hopping mechanisms can be precisely reflected by γ in organic semiconductors.[24,25] Although the power-law μ_{int} expression seems to be a general form for bulk semiconductors, its applicability to 2D semiconductors is yet to be verified.

Given that a wide variety of 2D materials are available for semiconducting channels, it is imperative to establish a generic extraction method that can precisely capture the intrinsic properties of these 2D semiconductors. A universal method for parameter extraction in 2D FETs is, therefore, developed in this work. The concept of the *F*-function method is employed, in which the characteristic temperature (T_o), threshold voltage (V_T), R_{SD}, and μ_{int} can be accurately extracted.[20,21] It is demonstrated that the proposed method is capable of characterizing the temperature-dependent carrier conduction mechanisms and the strain-induced band structure modification in 2D semiconductors. Different extraction techniques are compared with the best accuracy achieved by the proposed method. The precision is systematically verified by technology computer aided design (TCAD) analysis, and the simulation results show that not only a high resolution of R_{SD} extraction can be attained, but the other extracted parameters (T_o, V_T, and μ_{int}) are practically immune to the presence of substantial R_{SD} effects. Moreover, the universality of the proposed extraction method is validated by adequately implementing the extraction procedure to various 2D semiconductors with top- and bottom-gated configurations. This study offers an accurate yet simple method to probe the metal-2D semiconductor contact behaviors and the intrinsic properties in 2D FETs.

2. Universal Extraction Method

2.1. Power-Law Mobility Expression

The key aspect that determines the precision of extraction results is the presumption of the mobility expression as a function of gate voltage (V_G). A universal mobility expression is highly desired to accommodate complex conduction mechanisms in 2D semiconductors. A versatile power-law mobility expression is, therefore, utilized to model the intrinsic charge carrier mobility (μ_{int}) in 2D semiconductors, as shown in Equation (1).

$$\mu_{int(x)} = \mu_o \left(V_G - V_T - mV_x\right)^\gamma \quad (1)$$

where μ_o is the prefactor, V_T is the threshold voltage, V_x is the additional voltage drop at any given point x in the channel from the applied drain bias (V_D), and γ is the mobility dependency factor. If $\gamma > 0$, the carrier conduction is dominated by tail-distributed traps (TDTs) and/or variable range hopping (VRH), whereas the transport behavior is mainly governed by surface and/or phonon scattering effects if $-1 > \gamma > 0$.[23–27] Note that 2D FETs mostly operate in the accumulation mode, meaning that the depletion capacitance is negligible, so Equation (1) can be further simplified as $m = 1$.[28]

2.2. Generic Drain Current Equation

The drift-diffusion current equation is written as Equation (2.1), in which the diffusion current component can be neglected if the applied V_D is sufficiently small (i.e., $V_D \leq 0.1$ V), as shown in Equation (2.2).

$$J_{(x)} = -n_{(x)}\, q\mu_{int(x)} \frac{dV_{(x)}}{dx} - qD_{(x)} \frac{dn_{(x)}}{dx} \quad (2.1)$$

$$\approx -n_{(x)} q\mu_{int(x)} \frac{dV_{(x)}}{dx} \quad (2.2)$$

By integrating Equation (2.2) from source ($x = 0$) to drain side of the channel ($x = L$) with the substitution of $\mu_{int(x)}$ and $n_{(x)}$, one can obtain Equation (3) as

$$\int_0^L WI_{D(x)}\, dx = -\int_{V_s}^{V_d} C_{ox} \left(V_G - V_T - V_x\right)^{1+\gamma} dV_{(x)} \quad (3)$$

where W is the channel width, $I_{D(x)}$ is the drain current, and C_{ox} is the oxide capacitance per unit area. If the R_{SD} at source/drain (S/D) is negligible, V_s and V_d can be simplified as 0 and V_D, respectively. Additional voltage drop at the contact region has to be, however, accounted in the practical scenario where we assume that the total R_{SD} is the sum of those at the source (R_S) and drain (R_D) regions with R_S equals to R_D. Accordingly, taking into consideration the specific mobility behavior and R_{SD} effect, the generic drain current equation under thermal equilibrium can be derived as shown in Equation (4).

$$I_D = \frac{W}{L} \mu_o C_{ox} \left(V_G - V_T\right)^{2+\gamma} \left[\frac{\left(1 - \frac{V_s}{V_G - V_T}\right)^{2+\gamma} - \left(1 - \frac{V_d}{V_G - V_T}\right)^{2+\gamma}}{2+\gamma}\right] \quad (4)$$

To facilitate the parameter extraction, it is necessary to apply a regional approximation that simplifies the generic drain current expression. Note that the intrinsic properties of 2D materials

© 2021 The Authors. Advanced Functional Materials published by Wiley-VCH GmbH

can be best captured when operating 2D FETs under linear region. To this end, Equation (4) is approximated in which the sum of $V_s\left(\frac{I_D R_{SD}}{2}\right)$ and $V_d\left(V_D-\frac{I_D R_{SD}}{2}\right)$ is assumed to be much smaller than V_G–V_T. The binomial approximation can, therefore, be applied that reduces Equation (4) to

$$I_D=\frac{\frac{W}{L}\mu_o C_{ox}(V_G-V_T)^{1+\gamma}V_D}{1+\frac{W}{L}\mu_o C_{ox}(V_G-V_T)^{1+\gamma}R_{SD}} \quad (5)$$

The resultant Equation (5) resembles the mobility expression in the Y-function method but with an additional power term of γ.

2.3. Parameter Extraction Procedure

Y-function method (or ration method) has been commonly applied to extract μL_F and R_{SD} independently from a single device configuration, in which the mobility expression has been specifically modeled as $\mu_{int}=\frac{\mu_{LF}}{1+\theta_o(V_G-V_T)}$.[17,18] However, this expression may not be generally applicable to different material systems, which subsequently makes the Y-function method questionable. In fact, by utilizing the generic drain current equation from Equation (5), one can obtain the universal form of Y-function as

$$Y\equiv\frac{I_D}{\sqrt{g_m V_D}}=\sqrt{\frac{\frac{W}{L}\mu_o C_{ox}}{1+\gamma}}(V_G-V_T)^{1+\gamma/2} \quad (6)$$

where g_m is the transconductance defined as dI_D/dV_G. Although the R_{SD} effect can be eliminated by Y-function, Equation (6) is a linear function only when $\gamma = 0$, indicating that linear regression is not generally applicable. The concept of H-function, also known as the integration method, is subsequently employed for which the power-law function of Equation (6) can be reduced to a linear function as[19]

$$H(Y)\equiv\frac{\int_{-\infty}^{V_G}Ydx}{Y}=\frac{1}{2+\gamma/2}(V_G-V_T) \quad (7)$$

By extrapolating the calculated $H(Y)$ to V_G, one can obtain the power term of γ from slope. The generic Y-function expression can be further linearized as Equation (8), provided that γ has been determined from the slope of $H(Y)$–V_G plot in the previous step.

$$Y^{1/1+\frac{\gamma}{2}}=\frac{\int_{-\infty}^{V_G}Ydx}{Y}=\sqrt[2+\gamma]{\frac{\frac{W}{L}\mu_o C_{ox}}{1+\gamma}}(V_G-V_T) \quad (8)$$

From Equation (8), μ_0 and V_T can be extracted from the slope and x-intercept of the linear regression of $Y^{1/(1+0.5\gamma)}$ against V_G, respectively. Moreover, the R_{SD} value can be estimated from Equation (5) since R_{SD} is the only unknown parameter left, and μ_{int} can be ultimately determined without the influence of R_{SD} effects.

The above derivation combines the advantage of ration (Y-function) and integration (H-function) methods that not only eliminates the R_{SD} effect but preserves the linearity of the fitting function, which is desirable for the parameter extraction. In the following sections, the applicability of the present method will be comprehensively discussed and verified.

3. Results and Discussion

3.1. Characterization of the Temperature-Dependent Carrier Conduction

Temperature dependent measurement is one of the essential steps to assess the underlying device physics in 2D FETs, including carrier conduction through the semiconducting layer and at the metal-2D interface. It is crucial that the developed technique must be capable of characterizing the temperature effects on both channel and contact regions. In this section, temperature-dependent measurements are performed using top-gated nanoribbon black phosphorus (NR-BP) FET to evaluate the applicability of the proposed method. An array (×9) of 200 nm wide of nanoribbons is formed by deep reactive ion etching with the profile shown in the inset of **Figure 1**a. The transfer characteristics (I_D–V_G) of NR-BP FET are measured from a cryogenic temperature of 3–300 K at V_D = 0.1 V, as shown in Figure 1a. First, $H(Y)$ function is calculated from the experimental results throughout the entire temperature range (Section S1, Supporting Information). Good linear fittings are attained in Figure 1b, which indicate that the power term of γ as a function of temperature (T) can be determined from the slope of Equation (7). μ_o and V_T are subsequently obtained from the slope and x-intercept of Equation (8), respectively, as shown in Figure 1b. The characteristic temperature (T_o) of the density of states (DOS) in the forbidden band can be translated from $\gamma(T)$ by[23–25,29]

$$\gamma(Y)=2\left(\frac{T_o}{T}-1\right) \quad (9)$$

where the extracted T_o with respect to T is shown in Figure 1c. A linear correlation is observed between T_o and T, identifying the U-shape subgap states that is in good agreement with previous reports, as depicted in the inset of Figure 1c.[30–35] This result demonstrates that the present method is capable of probing the profile of defect states in 2D FETs. Note that Equation (8) is generally applicable to thermal-activated conductions, including the tail-distributed states (TDTs) and the hopping conduction through the percolation path.[23–25]

Given that γ, V_T, and μ_o have been obtained from the above procedure, the total R_{SD} and intrinsic mobility (μ_{int}) can be, thus, extracted from Equations (5) and (1), respectively, as shown in Figure 1d. Note that R_{SD} decreases with increasing temperature, revealing a thermal-activated transport behavior at the metal-2D interface. On the other hand, μ_{int} increases with the ambient temperature that is in good agreement with the defect-dominated carrier conduction in the semiconducting

© 2021 The Authors. Advanced Functional Materials published by Wiley-VCH GmbH

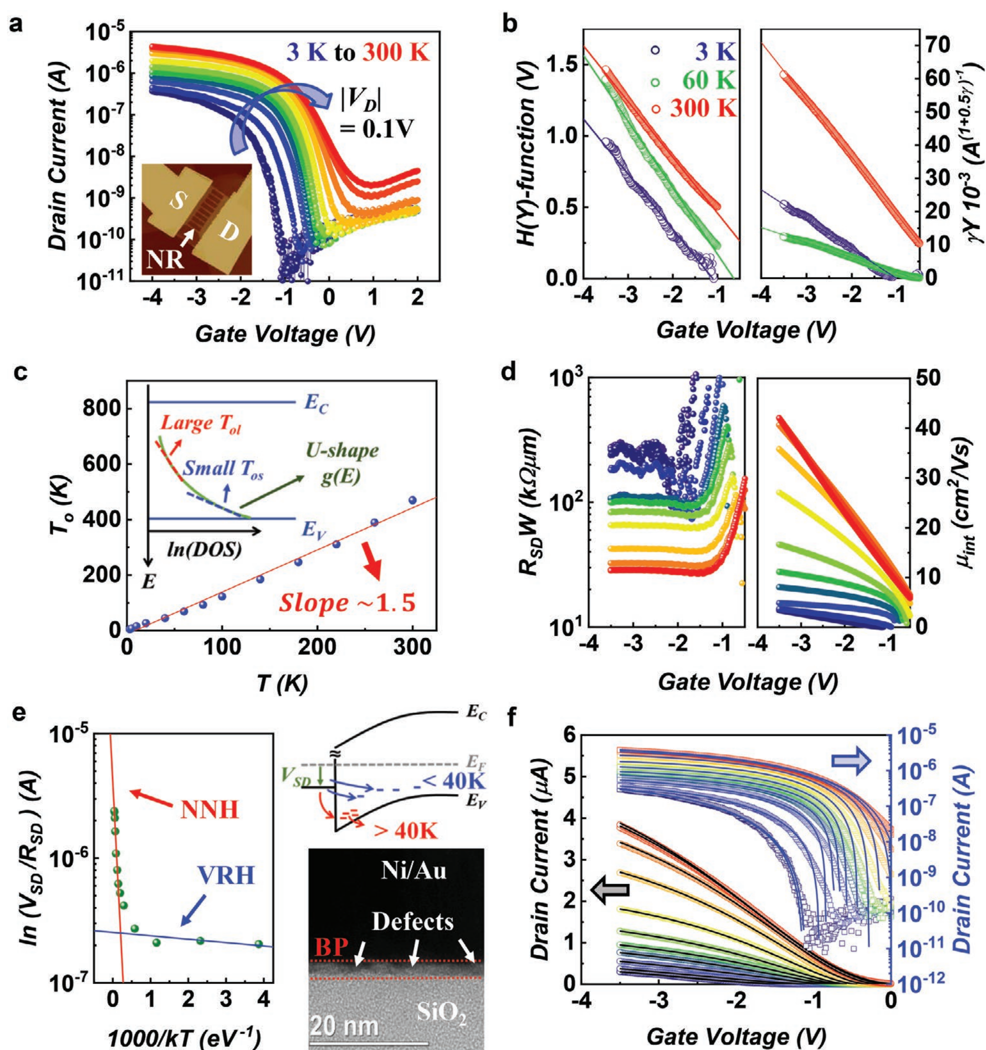

Figure 1. a) Temperature-dependent I_D–V_G curves of NR-BP FET from the cryogenic temperature of 3–300 K at V_D = 0.1 V. The inset shows the top view of a 200 nm wide (×9) NR-BP FET by atomic force microscopy. b) Linear regression of the $H(Y)$ and γY functions to V_G at T = 3, 60, and 300 K. c) Extracted T_o as a function of T. The linear correlation with a slope of 1.5 indicates a U-shape distributed defect states in the forbidden band illustrated in the inset. The U-shape distributed defect states can be described by the summation of the exponential density of states with different T_o as $g(E) = \sum_{i=1}^{i=n} g_{ci} \exp(-\Delta E/kT_{oi})$. ΔE is the absolute energy difference between the valence band edge (E_v) and the defect level (E_{it}). d) Temperature-dependent R_{SD} and μ_{int} from 3 K (purple dots) to 300 K (red dots). e) Arrhenius plot at the contact region with the fitted nearest neighbor hopping (>40 K) and variable range hopping (<40 K) mechanisms. The energy band diagram depicts that carriers inject via the defect states at the interface. Defects between the metal-2D interface can be evidenced by the cross-section image from transmission electron microscopy. f) Comparison between the experimental (dots) and simulated (lines) results with linear (left x-axis) and logarithmic (right x-axis) scale from T = 3 K (purple) to T = 300 K (red) at V_D = 0.1 V.

channel. To further explore the conduction mechanisms at the metal-2D interface, the Arrhenius plot is created specifically at the contact region, as shown in Figure 1e. Two distinct transport behaviors can be clearly observed in which the nearest neighbor hopping (NNH) and variable range hopping (VRH) can be best fitted and described for the high and low temperature regimes, respectively, with the transition temperature at 40 K. Observation of the transition between NNH and VRH at the low temperature condition (≈40 K) is compatible with the fundamental physics of VRH, where the lowest hopping distance is preferred when the carriers possess low thermal energy, resulting in variable hopping distances.[24,25,36]

Moreover, the hopping conduction occurs owing to the presence of defect states at the metal-2D interface, which can be further evidenced by the cross-section image at the contact region from transmission electron microscopy (TEM), as shown in Figure 1e.[37] The identification of the hopping conduction from the temperature-dependent R_{SD} highlights the precision of the proposed technique to unravel the carrier injection at the metal-2D interface.

A final confirmation to verify the extracted parameters is to compare the simulated transfer characteristics (I_D–V_G) with those from measurements, in which the simulation results are constructed by Equation (5) from the extracted parameters,

© 2021 The Authors. Advanced Functional Materials published by Wiley-VCH GmbH

including γ, V_T, μ_o, R_{SD}, and μ_{int}. Figure 1f shows the comparison of the simulated and experimental I_D–V_G curves, which demonstrates high precision for the entire measurement conditions (T = 3–300 K) with an error of <1%. In addition, the V_G-independent R_{SD} (see Figure 1d) in the above threshold region (V_G >> V_T) serves as a strong indicator of the reliability of our assumptions made in the model derivation, such as the power-law mobility expression and the constant R_{SD} at a given ambient condition.

3.2. Comparison between Different Extraction Techniques

3.2.1. Transconductance Method

Apart from the method described in this article, various extraction techniques have been proposed to extract μ_{int} and/or R_{SD} from a standalone device. One of the most commonly employed methods is the transconductance (g_m) method, where the so-called field-effect mobility (μ_{FE}) is estimated by Equation (10).[11,38–40]

$$\mu_{FE} = \frac{\partial I_D}{\partial V_G}\ \frac{L}{WC_{ox}V_D} = \frac{g_m L}{WC_{ox}V_D} \tag{10}$$

A noticeable flaw in the g_m method is the negligence of R_{SD} that overestimates the lateral voltage drop across the channel region, resulting in an underestimation of the charge carrier mobility, as shown in the blue curve of **Figure 2**a. Moreover, Equation (10) implicitly assumes a constant charge carrier mobility with respect to V_G, in which the additional differential term of $\partial\mu/\partial V_G$ is completely omitted (Section S2, Supporting Information). This creates a prominent error (>200%) on the estimation of μ_{FE} even when the R_{SD} effect has been fully calibrated, as shown in the red curve of Figure 2a. The extend of extraction error is closely related to the term of $\partial\mu/\partial V_G$. The aforementioned results emphasize that the g_m method should not be a standard method to estimate the charge carrier mobility because the R_{SD} value cannot be extracted purely by this technique, and the negligence of V_G-dependent charge carrier mobility substantially generates a considerable error on the evaluation of μ_{FE}.

3.2.2. Resistance Extrapolation Method

The resistance extrapolation method is an intuitive approach to determine R_{SD}. The R_{SD} is estimated by linearly extrapolating the total resistance (R_o) to the infinite value of V_G–V_T, at which the channel resistance (R_{ch}) becomes negligible. Note that the determination of threshold voltage (V_T) is required to perform linear regression, where the erroneous extraction can be easily introduced in this step. Indeed, negative R_{SD} has been obtained from this method, as shown in Figure 2b, regardless of the input V_T from different methods (e.g., maximum g_m method and constant current method).[41,42] In addition, the resistance extrapolation method inherently assumes a constant charge carrier mobility that could further aggravate the extraction errors.

3.2.3. Asymptotical Method

The asymptotical method relies on the asymptotical behavior of R_o that gradually decreases with V_G, and R_o eventually saturates at a certain condition when V_G is sufficiently large, and the respective resistance is taken as the value of R_{SD}.[15,16,43,44] This method eliminates the presumption of a constant charge carrier mobility and the determination of V_T that possesses higher flexibility than the resistance extrapolation method. The primary concern of the asymptotical method is its lack of physical interpretation that hinders the selection of a proper asymptotical function to fit the experimental results, as indicated in Figure 2c. Exponential and polynomial functions have been employed to determine the R_{SD} value, in which a significant deviation can be clearly seen on the calculation of R_{SD} from different fitting functions, although good fittings can be acquired for all the functions. Details on the fitting parameters can be found in Section S3, Supporting Information. This observation can be attributed to the lack of physical explanations in the asymptotical method, despite that the second-order polynomial function seems to best reproduce the extracted R_{SD}, as compared to our proposed method.

It is noteworthy that the closely approximated R_{SD} value from the polynomial function could be attributed to the similarity with the drain current equation in which R_o is proportional to the reciprocal form of the V_G–V_T term, as indicated in Equation (5). On the other hand, the rapid decrease nature of the exponential function overrates the gate tunability to R_o, which consequently requires a significant intercept value (γ_o) to balance with the experimental measurements (Section S3, Table S1, Supporting Information), clarifying the origin of the overestimation of R_{SD} value from the exponential functions.

3.2.4. Y-function Method

Y-function method or the ratio method, defined as $Y = I_D/g_m$, has been widely employed to extract the low field mobility (μL_F) and R_{SD}.[17,18] This method has been first proposed to characterize Si MOSFETs, in which the analytical expression of μ_{int} has been explicitly modeled by

$$\mu_{int} = \frac{\mu_{LF}}{1+\theta_o\left(V_G - V_T\right)} \tag{11}$$

where θ_o is the mobility attenuation factor that can be related to the scattering events in the semiconducting channel.[26,27] Details of the extraction procedure on μ_{int}, V_T, and R_{SD} are described in Section S4, Supporting Information. Although the Y-function method has been applied in 2D FETs, the suitability of Equation (11) in 2D FETs remains unclear given that the scattering effects are not the only dominating mechanism in 2D semiconductors (i.e., defect-dominated conduction).[29,35] In fact, the non-linear behavior of Y-function with respect to V_G as shown in Figure 2d specifies that the above μ_{int} expression is not generically applicable to 2D FETs, and the extracted R_{SD} could be inevitably overestimated by this method (Section S4, Supporting Information).

© 2021 The Authors. Advanced Functional Materials published by Wiley-VCH GmbH

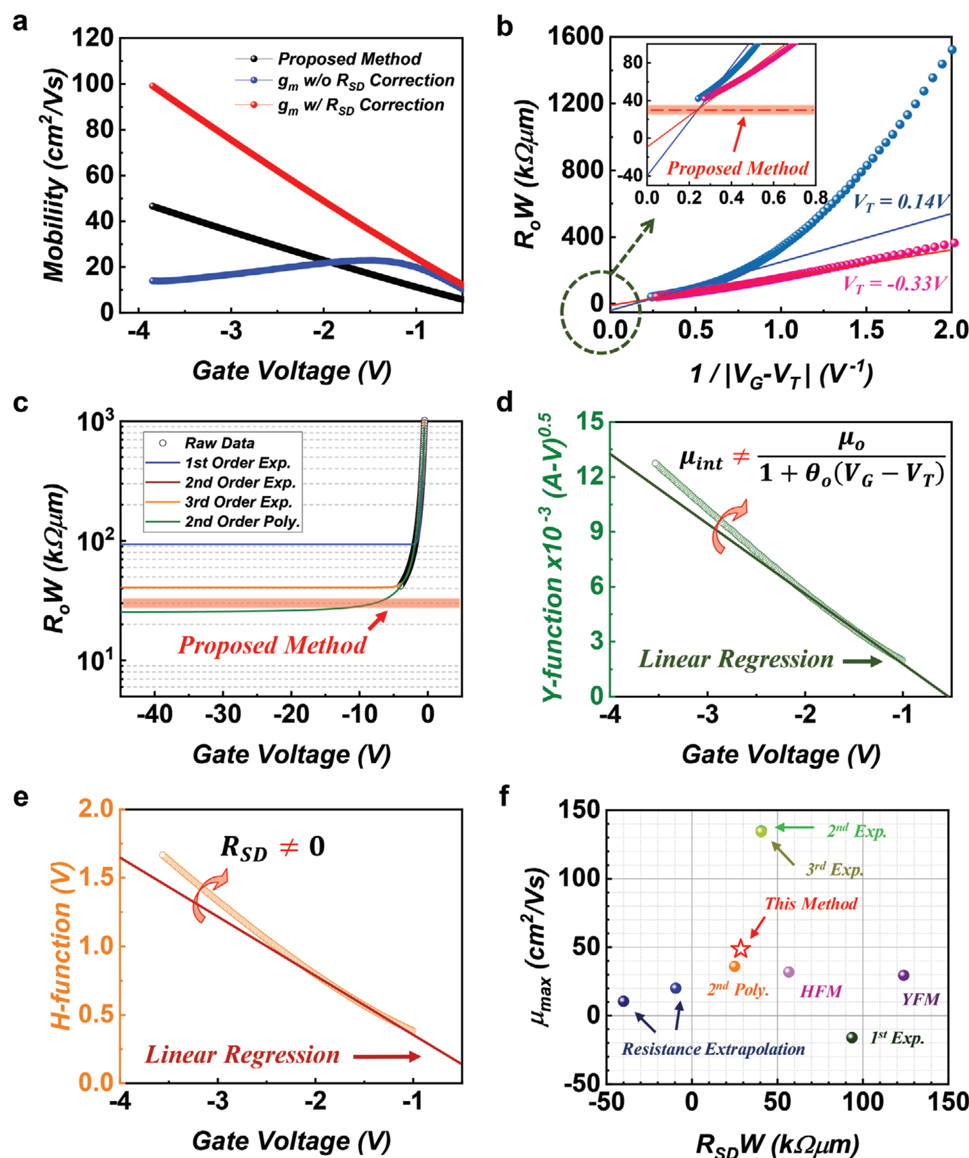

Figure 2. a) Extracted charge carrier mobility from the proposed method (black), g_m method w/o R_{SD} correction (blue), and g_m method w/R_{SD} correction (red). R_{SD} is estimated by the proposed method. b) R_o as a function of the absolute reciprocal of V_G–V_T. $V_T = 0.14$ and –0.33 V are determined by constant current and maximum g_m methods, respectively. The inset shows the enlarged scale in the vicinity of the *y*-intercept. c) Calculated R_o as a function of V_G with the asymptotical behavior fitted by 1st-order exponential (blue), 2nd-order exponential (brown), 3rd-order exponential (orange), and 2nd-order polynomial (green) functions. d) *Y*-function and e) *H*-function method for parameter extraction with the referenced linear regression. f) Benchmarking of the extracted μm_{ax} and R_{SD} from different techniques.

3.2.5. H-function Method

H-function method or the integration method is an alternative approach to account for the defect- and/or scattering-dominated carrier conduction where the analytical charge carrier mobility expression is defined as $\mu_{int} = \mu_o(V_G - V_T)^\gamma$ that resembles Equation (1) but without the consideration of R_{SD} effects.[19] *H*-function is then defined as

$$H \equiv \frac{\int_{-\infty}^{V_G} I_D dV_G}{I_D} = \frac{1}{2+\gamma}(V_G - V_T) \tag{12}$$

The γ and V_T can be extracted from the slope and *x*-intercept of the linear regression of the H–V_G curve (Figure 2e), and R_{SD} is then iterated with the details described in Section S5, Supporting Information. Note that the *H*-function method first omits the R_{SD} effects in the extraction of γ and V_T but subsequently calculates the R_{SD} value between the difference of total resistance and the extracted channel resistance as $R_{ch} = \frac{L}{W\mu_o C_{ox}(V_G - V_T)^{1+\gamma}}$.[19] However, the non-linear correlation between H and V_G highlights that the negligence of R_{SD} is not feasible, suggesting that an extraction error can still be introduced by the *H*-function method.

 © 2021 The Authors. Advanced Functional Materials published by Wiley-VCH GmbH

3.2.6. Comparison of the Extracted Results between Different Techniques

Figure 2f shows the extracted R_{SD} and maximum intrinsic charge carrier mobility (μ_{max}) from various extraction techniques described in the above sections, including resistance extrapolation, asymptotical behavior, *Y*-function, and *H*-function methods. The resistance extrapolation method provides an unreasonable value of R_{SD}, which can be attributed to the numerous errors introduced by the assumption of a constant μ_{int} and the determination of V_T. Although a higher extraction accuracy of R_{SD} can be attained from the second-order polynomial function of the asymptotical method, its lack of underlying physics makes this method questionable. Analytical methods, such as the *Y*-function and *H*-function methods, oversimplify the practical scenario of the carrier conduction in 2D FETs, which can unintentionally lead to erroneous extractions. In contrast, our proposed method offers the best accuracy among these extraction techniques, and this argument can be further supported by the excellent agreement between the simulation and the experimental results (see Figure 1f).

3.3. Capture of the Strain-Induced Bandgap Modification

Strain-induced band structure modification is another interesting aspect in 2D semiconductors that has recently gained significant attention.[45–50] Given that the atomically thin nature of 2D materials, these semiconductors are expected to be highly sensitive to external stress. The variation of the band structures can consequently alter the carrier conduction and the defect distribution in 2D semiconductors. Indeed, it has been discovered by several reports that the performance of 2D FETs can be substantially improved by adequately introducing the strain effect.[47,50] An accurate yet practical extraction technique must be able to characterize the conduction mechanisms arising from the external strain effects. In this section, we demonstrate that the present extraction method is capable of unraveling the underlying device physics arising from strain-induced band structure modification in 2D semiconductors with the utilization of a flexible top-gated indium selenide (InSe) FET as a vehicle for the discussion.

Figure 3a,b show the I_D–V_G curves under compressive strain (CS) and tensile strain (TS) at 300 K with different strain levels (ε), respectively. Notably, the on-state I_D decreases with the application of CS, whereas I_D increases with the exertion of TS. This observation demonstrates that the applied strain effect indeed affects the electronic property of 2D semiconductors, and the type of strain is crucial to determine its performance. However, the dominating mechanism responsible for this phenomenon remains unclear, and it is unfair to simply account this observation for the change of charge carrier mobility in 2D semiconductors. The method developed in this study is, therefore, implemented to explore the underlying device physics in both channel and contact areas. Linear regression of $H(Y)$ and γY functions with various ε are performed in Figure 3c where the good linear fitting ensures the reliability of R_{SD} and μ_{int} extraction, as shown in Figure 3d,e, respectively (Section S6, Supporting Information). It can be seen from Figure 3d that R_{SD} decreases with the introduction of TS, and the extracted R_{SD} with respect to the ε level is shown in Section S7, Supporting Information. We would like to argue that the strain-dependent R_{SD} behavior has not been explored much in 2D FETs, although it is an imperative aspect to understand the carrier injection through the metal-semiconductor interface. On the other hand, the extracted μ_{int}, shown in Figure 3e, reveals two distinct mechanisms where the μ_{int} decreases and increases with the application of TS ($\varepsilon > 0\%$) at $V_G = 2$ V (low-bias regime) and $V_G = 5$ V (high-bias regime), respectively. The complete μ_{int}–V_G curves with various ε levels can be found in Section S7, Supporting Information. Moreover, the extracted T_o reflects a similar behavior with the subthreshold slope (*S.S.*) in respect of ε, as shown in Figure 3f.

Based on the aforementioned extraction results, one can unambiguously confirm that the strain effect not only alters the carrier conduction in the above-threshold regime but rearranges the profile of defect distribution in the forbidden band (e.g., the extracted T_o). Accordingly, the energy band diagram is proposed to clarify the strain-induced band structure modification, as shown in Figure 3g. At $\varepsilon = 0\%$, the effective kT_o of 50 meV is depicted according to the extraction results shown in Figure 3f, representing the profile of defect states in the forbidden band. When $\varepsilon < 0\%$, the reduction of trap states with shallow distribution ($kT_o = 45$ meV) can be elucidated by the extracted *S.S.* and μ_{int} at the low-bias region (i.e., $V_G = 2$ V). The bandgap (E_g) of InSe increases with the application of CS ($\varepsilon < 0\%$) that is responsible for the enhancement of R_{SD} and the reduction of μ_{int} at the high-bias region (i.e., $V_G = 5$ V), as shown in Figure 3d,e, respectively. In contrast, E_g decreases with the application of TS ($\varepsilon > 0\%$), and trap state increases when TS is applied ($\varepsilon > 0\%$), which can be supported by the extracted R_{SD}, μ_{int}, and kT_o. The observation of strain-dependent E_g to ε is in good agreement with those from the first-principle calculation, clarifying that the proposed extraction method is applicable to capture the intrinsic properties of 2D semiconductors.[48–50]

To verify the accuracy of the extracted parameters, Figure 3h shows the comparison between the experimental and simulated results under different ε. The simulation curves are constructed by Equation (5) with the parameters extracted using the proposed method (γ, μ_o, V_T, μ_{int}, and R_{SD}). A good match has been successfully attained not only for I_D, but the g_m virtually displays no deviation between measurements and simulations. These results comprehensively demonstrate the precision of the parameter extraction from the present method.

3.4. Universality on 2D FETs

In previous sections, it has been demonstrated that our proposed method is feasible to accurately account for the temperature- and strain-dependent effects on 2D FETs. In this section, simulation studies are further carried out to examine its applicability on 2D FETs, namely the resolution limits on the extracted parameters. In addition, the universality of the current method on the characterization of 2D FETs will be demonstrated by various 2D semiconductors with top- and bottom-gated configurations.

© 2021 The Authors. Advanced Functional Materials published by Wiley-VCH GmbH

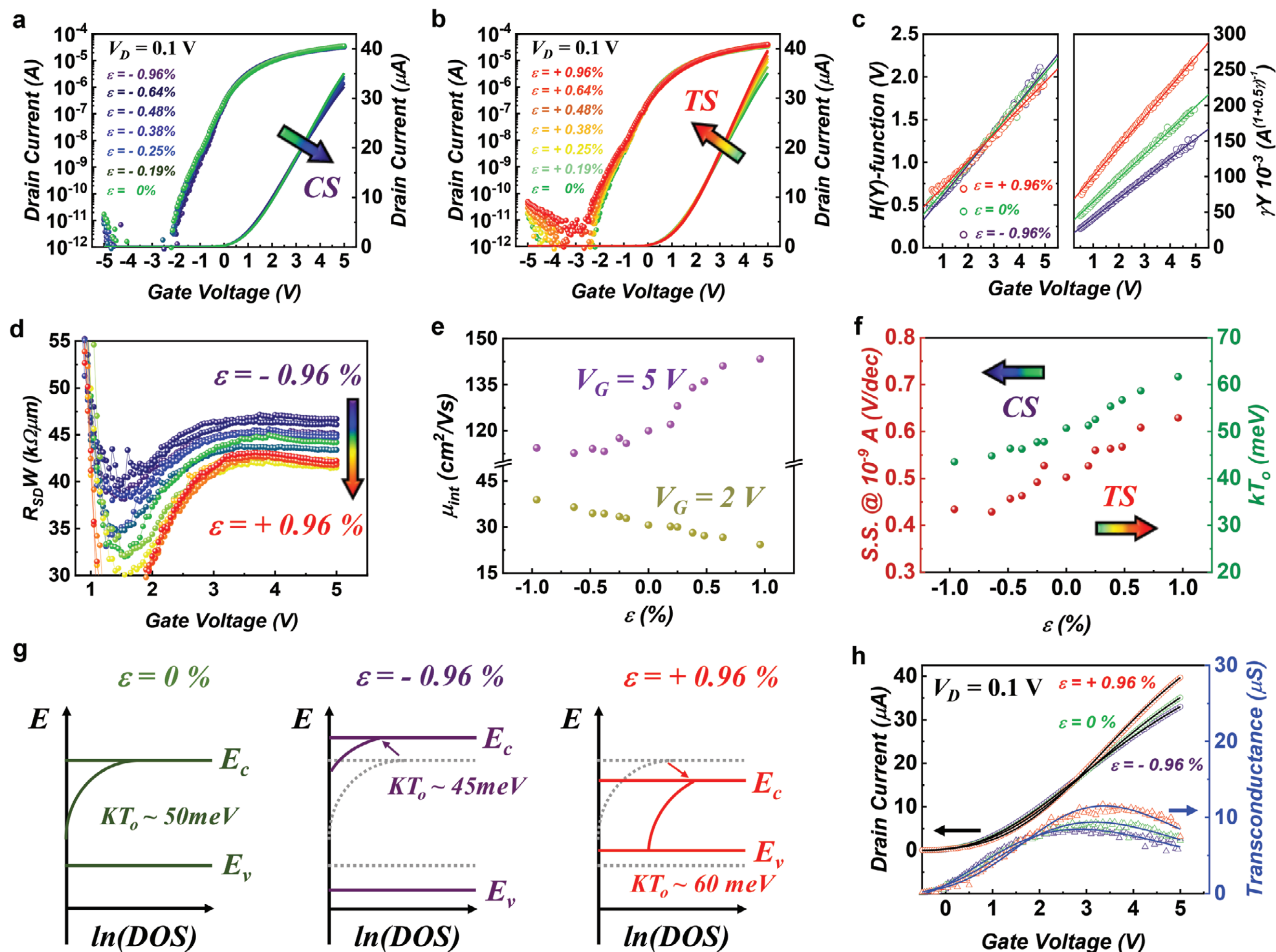

Figure 3. I_D–V_G curves for InSe FET under a) CS and b) TS condition with various strain levels (ε) at $V_D = 0.1$ V. c) Linear regression of the $H(Y)$ and γY functions with respect to V_G at $\varepsilon = -0.96\%$ (purple), 0% (green), and + 0.96% (red). d) Extracted R_{SD}–V_G curves under different ε. e) The extracted μ_{int} decreases and increases with ε at $V_G = 2$ V and $V_G = 5$ V, respectively, demonstrating two distinctive conduction mechanisms. f) Calculated $S.S.$ at I_D of 10^{-9} A and kT_o with respect to ε. g) Illustration of the strain-induced band structure variation with the change of defect distribution in the forbidden band at different strain levels. h) Comparison between the experimental (dots) and simulated (lines) results with the linear scale of drain current (left *x*-axis) and transconductance (right *x*-axis) at $V_D = 0.1$ V.

Commonly, the characterization of the intrinsic properties in 2D semiconductors, such as the charge carrier mobility, can be inevitably affected by the presence of the R_{SD} effect. Therefore, it is necessary to verify that the proposed method is practically immune to these external factors. **Figure 4**a shows the theoretically extracted parameters as a function of the input R_{SD} values from 0.1 to 20 kΩ. One can clearly observe that the extracted parameters, including kT_o, V_T, μ_o, and μ_{int}, are nearly independent of the input R_{SD} values, demonstrating the feasibility of the current method in eliminating the R_{SD} effects. On the other hand, the resolution on the extraction of R_{SD} is an imperative aspect in determining the universality of the proposed technique, as 2D FETs possess a diverse contact behavior. TCAD simulation is, therefore, employed to verify the sensitivity of the R_{SD} extraction, in which the R_{SD} at the metal-semiconductor interface and the defect distribution in the semiconducting channel are the controlled factors to construct the simulated I_D–V_G characteristics. Details on the simulation procedure can be found in Section S8, Supporting Information. To account for the distinctive properties of 2D semiconductors and the corresponding contact behavior in TCAD simulation, the input values, namely the R_{SD} value and the profile of defect states, are substantially varied, as shown in Figure 4b. It can be observed that the extracted R_{SD} nearly exhibits an identical input value with a slope of one, unarguably manifesting that our proposed method is capable of accommodating various R_{SD} values while preserving the extraction accuracy.

Moreover, the method has been extensively applied to various elemental and transition metal dichalcogenide channels with different configurations, including NR-BP, planar BP, InSe, chemical vapored deposited molybdenum disulfide (CVD-MoS_2), MoS_2, rhenium disulfide (ReS_2), and tungsten disulfide (WS_2), to validate the universality of the proposed model. One can observe that the extracted parameters are consistent with those from experiments (extraction details in Section S9, Supporting Information), in which the simulated I_D-V_G curves

© 2021 The Authors. Advanced Functional Materials published by Wiley-VCH GmbH

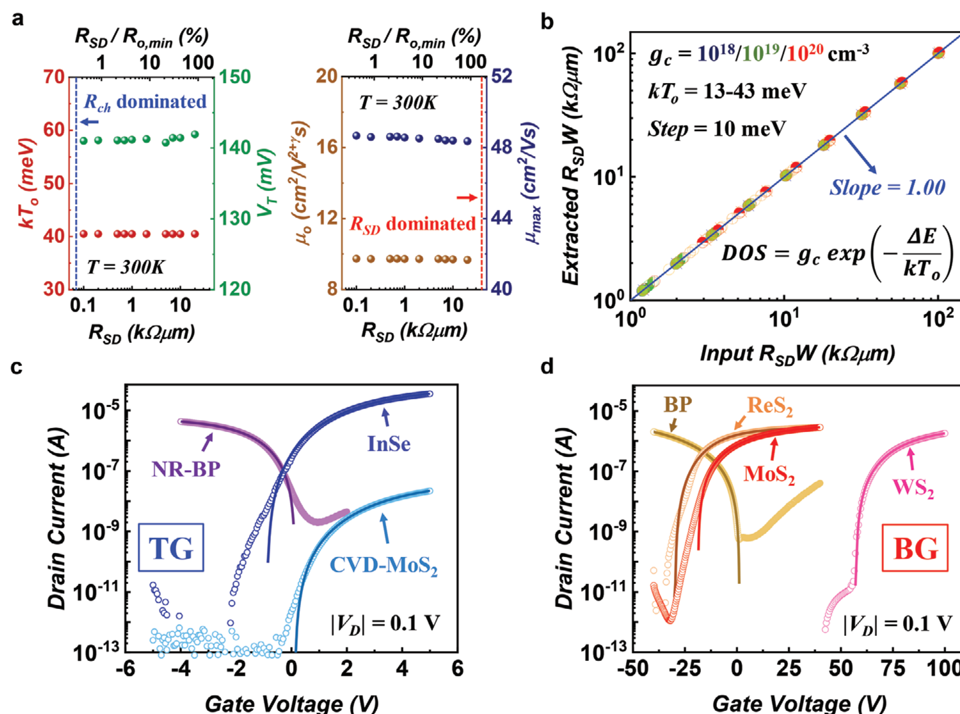

Figure 4. a) Simulated extraction results of kT_o, V_T, μ_o, and μm_{ax} as a function of R_{SD} from 0.1 kΩ µm (channel dominated conduction) to 20 kΩ µm (contact dominated conduction). b) Comparison of the simulated R_{SD} extraction results with the input R_{SD} value from TCAD analysis with different profiles of the density of states (DOS) in the forbidden band of the semiconducting channel ($g_c = 10^{18}/10^{19}/10^{20}$ cm^{-3} and kT_o = 13/23/33/43 meV). g_c is the defect density at the conduction band edge, and ΔE is the energy difference between the conduction band edge and the defect level. A linear correlation is obtained with a slope of one. Measured (dot) and modeled (line) I_D–V_G curves of various 2D FETs at $|V_D/ = 0.1$ V with c) top (TG) and d) bottom gate (BG) configurations. The modeled curves are constructed by Equation (5) with the parameters extracted from the proposed method.

are in excellent agreement with those from measurements in the above threshold regime ($V_G >> V_T$) for both top- and bottom-gated structures, as shown in Figure 4c,d, respectively. These results reinforce that the proposed method is not only accurate to characterize the intrinsic parameters in 2D FETs but also universally applicable to 2D semiconducting materials.

4. Conclusion

A versatile extraction method to accurately characterize the performance of 2D FETs using a simple I_D–V_G curve was developed. The temperature-dependent electrical performance and the strain-induced band structure modification were successfully characterized by the proposed extraction method. The accuracy of the extraction method was confirmed by fitting the extracted parameters with those from measurements. The resolution limit was clarified by employing the TCAD simulation that showed an accurate R_{SD} extraction over a two-order magnitude of difference. In addition, the intrinsic parameters, such as T_o, V_T, and μ_{int}, were virtually immune to the presence of the R_{SD} effect. The universality of this method was proven by extending the extraction procedure to various elemental and transition metal dichalcogenide channels with different gate configurations. In conclusion, we showed the applicability of the proposed method for unveiling the intrinsic properties of 2D FETs and their underlying device physics.

5. Experimental Section

2D FETs with various elemental and transition metal dichalcogenide channels were experimentally demonstrated. TG NR-BP FET was fabricated on a SiO_2/Si substrate with 20 nm of aluminum oxide (Al_2O_3) as the gate oxide and 3/40 nm of nickel (Ni)/gold (Au) as the contact metal. Details on the fabrication of nanoribbon structure are described elsewhere.[44] TG indium selenide (InSe) was prepared by mechanical exfoliation on a polyimide substrate with 30 nm of Al_2O_3 as the gate oxide and 20/100 nm of chromium (Cr)/Au as the contact metal.[44] TG CVD-MoS_2 was integrated on a sapphire substrate with 20nm of hafnium oxide (HfO_2) as the gate oxide and 5/70 nm of titanium (Ti)/Au as the contact metal. BG devices, namely planar BP, MoS_2, ReS_2, and WS_2, were fabricated by mechanical exfoliation on a heavily doped silicon oxide (SiO_2)/Si global gate stack with the contact metal of 3/40 nm Ni/Au, 40 nm Ni, 10/90 nm Ti/Au, and 3/50 nm of Ti/Au, respectively.[51,52] All the electrical measurements were performed at 300 K in a dark probe station under ambient conditions.

Supporting Information

Supporting Information is available from the Wiley Online Library or from the author.

Acknowledgements

Y.-C.C., X.F., and L.C. contributed equally to this work. This work is supported in part by National Research Foundation Competitive Research Programs (NRF-CRP24-2020-0002), in part by A*STAR

© 2021 The Authors. Advanced Functional Materials published by Wiley-VCH GmbH

Science and Engineering Research Council under its AME IRG Program (No. A2083c0061), in part by Ministry of Education Tier-2 Grant (MOE-T2EP50120-0016), and in part by the Applied Materials-NUS Advanced Corporate Laboratory Scholarship (A*STAR IAF-ICP I1801E0022).

Conflict of Interest

The authors declare no conflict of interest.

Data Availability Statement

The data that support the findings of this study are available from the corresponding author upon reasonable request.

Keywords

2D semiconductor field-effect transistors, charge carrier mobility, contact resistance, parameters extraction

Received: May 26, 2021
Revised: July 5, 2021
Published online:

[1] D. Akinwande, C. Huyghebaert, C. Wang, M. I. Serna, S. Goossens, L. Li, H. P. Wong, F. H. L. Koppens, *Nature* **2020**, *573*, 507.
[2] N. Oliva, J. Backman, L. Capua, M. Cavelieri, M. Luisier, A. M. Ionescu, *npj 2D Mater. Appl.* **2020**, *4*, 5.
[3] G. Nazir, M. A. Rehman, M. F. Khan, G. Dastgeer, S. Aftab, A. M. Afzal, Y. Seo, J. Eom, *ACS Appl. Mater. Interfaces* **2018**, *10*, 32501.
[4] I. Asselberghs, Q. Smets, T. Schram, B. Groven, D. Verreck, A. Afzalian, G. Arutchelvan, A. Gaur, D. Cott, T. Maurice, S. Brems, K. Kennes, A. Phommahaxay, E. Dupuy, D. Radisic, J. F. De Marneffe, A. Thiam, W. Li, K. Devriendt, C. Huyghebaert, D. Lin, M. Caymax, P. Morin, I. P. Radu, in *Int. Electron Devices Meet. IEDM*, IEEE, San Francisco, CA **2020**.
[5] Q. Smets, B. Groven, M. Caymax, I. Radu, G. Arutchelvan, J. Jussot, D. Verreck, I. Asselberghs, A. N. Mehta, A. Gaur, D. Lin, S. El Kazzi, in *Int. Electron Devices Meet. IEDM*, IEEE, San Francisco, CA, USA **2019**.
[6] K. Kang, S. Xie, L. Huang, Y. Han, P. Y. Huang, K. F. Mak, C. J. Kim, D. Muller, J. Park, *Nature* **2015**, *520*, 656.
[7] K. K. H. Smithe, S. V. Suryavanshi, M. Muñoz Rojo, A. D. Tedjarati, E. Pop, *ACS Nano* **2017**, *11*, 8456.
[8] W. Zhang, Z. Huang, W. Zhang, Y. Li, *Nano Res.* **2014**, *7*, 1731.
[9] W. Cao, J. Kang, D. Sarkar, W. Liu, K. Banerjee, *IEEE Trans. Electron Devices* **2015**, *62*, 3459.
[10] C. Klinkert, A. Szabo, C. Stieger, D. Campi, N. Marzari, M. Luisier, *ACS Nano* **2020**, *14*, 8605.
[11] Dieter K. Schroder, in *Semiconductor Material and Device Characterization*, 3rd Ed, Wiley-VCH, Weinheim, Germany **2006**, Ch. 3.
[12] Y. Liu, X. Duan, H. J. Shin, S. Park, Y. Huang, X. Duan, *Nature* **2021**, *591*, 43.
[13] C. Rolin, E. Kang, J. H. Lee, G. Borghs, P. Heremans, J. Genoe, *Nat. Commun.* **2017**, *8*, 14975.
[14] G. Nazir, M. F. Khan, V. M. Lermolenko, J. Eom, *RSC Adv.* **2016**, *6*, 60787.
[15] A. Dixit, A. Kottantharayil, N. Collaert, M. Goodwin, M. Jurczak, K. De Meyer, *IEEE Trans. Electron Dev.* **2005**, *52*, 1132.
[16] T. Roy, M. Tosun, J. S. Kang, A. B. Sachid, S. B. Desai, M. Hettick, C. C. Hu, A. Javey, *ACS Nano* **2014**, *8*, 6259.
[17] G. Ghibaudo, *Electron. Lett.* **1988**, *24*, 543
[18] H. Y. Chang, W. Zhu, D. Akinwande, *Appl. Phys. Lett.* **2014**, *104*, 113504.
[19] A. Cerdeira, M. Estrada, R. Garcia, A. Ortiz-Conde, F. J. Garcia Sanchez, *Solid. State. Electron.* **2001**, *45*, 1077.
[20] Z. Tang, M. S. Park, S. H. Jin, C. R. Wie, *IEEE Trans. Electron Devices* **2010**, *57*, 1093.
[21] O. Marinov, M. Jamal Deen, C. Feng, Y. Wu, *J. Appl. Phys.* **2014**, *115*, 034506.
[22] J. B. Kim, D. R. Lee, *Appl. Phys. Lett.* **2018**, *112*, 173301.
[23] M. Shur, M. Hack, *J. Appl. Phys.* **1984**, *55*, 3831.
[24] M. C. J. M. Vissenberg, M. Matters, *Phys. Rev. B* **1998**, *57*, 12964.
[25] O. Marinov, M. J. Deen, R. Datars, *J. Appl. Phys.* **2009**, *106*, 064501.
[26] G. Reichert, T. Ouisse, *IEEE Trans. Electron Devices* **1996**, *43*, 1394.
[27] F. Lime, K. Oshima, M. Cassé, G. Ghibaudo, S. Cristoloveanu, B. Guillaumot, H. Iwai, *Solid. State. Electron.* **2003**, *47*, 1617.
[28] Y. Taur, T. H. Ning, in *Fundamentals of Modern VLSI Devices*, 2nd Ed, Cambridge University Press, Cambridge, UK **2018**, Ch. 3.
[29] H. Qiu, T. Xu, Z. Wang, W. Ren, H. Nan, Z. Ni, Q. Chen, S. Yuan, F. Miao, F. Song, G. Long, Y. Shi, L. Sun, J. Wang, X. Wang, *Nat. Commun.* **2013**, *4*, 2642.
[30] A. Gaur, D. Chiappe, D. Lin, D. Cott, I. Asselberghs, M. Heyns, I. Radu, *2D Mater.* **2019**, *6*, 035035.
[31] A. Gaur, T. Agarwal, I. Asselberghs, I. Radu, M. Heyns, D. Lin, *2D Mater.* **2020**, *7*, 035018.
[32] P. Xia, X. Feng, R. J. Ng, S. Wang, D. Chi, C. Li, Z. He, X. Liu, K.-W. Ang, *Sci. Rep.* **2017**, *7*, 40669.
[33] W. Zhu, T. Low, Y. H. Lee, H. Wang, D. B. Farmer, J. Kong, F. Xia, P. Avouris, *Nat. Commun.* **2014**, *5*, 3087.
[34] P. Zhao, A. Khosravi, A. Azcatl, P. Bolshakov, G. Mirabelli, E. Caruso, C. L. Hinkle, P. K. Hurley, R. M. Wallace, C. D. Young, *2D Mater.* **2018**, *5*, 031002.
[35] N. Fang, S. Toyoda, T. Taniguchi, K. Watanabe, K. Nagashio, *Adv. Funct. Mater.* **2019**, *29*, 1904465.
[36] N. F. Mott, E. A. Davis, in *Electronic Processes in Non-Crystalline Materials*, 2nd Ed, Oxford University Press, Oxford, UK **2012**, Ch. 2.
[37] W. C. Tan, Y. Cai, R. J. Ng, L. Huang, X. Feng, G. Zhang, Y.-W. Zhang, C. A. Nijhuis, X. Liu, K.-W. Ang, *Adv. Mater.* **2017**, *29*, 1700503.
[38] M. S. Fuhrer, J. Hone, *Nat. Nanotechnol.* **2013**, *8*, 146.
[39] E. G. Bittle, J. I. Basham, T. N. Jackson, O. D. Jurchescu, D. J. Gundlach, *Nat. Commun.* **2016**, *7*, 10908.
[40] H. H. Choi, K. Cho, C. D. Frisbie, H. Sirringhaus, V. Podzorov, *Nat. Mater.* **2017**, *17*, 2.
[41] A. Ortiz-Conde, F. J. García-Sánchez, J. Muci, A. Terán Barrios, J. J. Liou, C. S. Ho, *Microelectron. Reliab.* **2013**, *53*, 90.
[42] A. Ortiz-Conde, A. Sucre-González, F. Zárate-Rincón, R. Torres-Torres, R. S. Murphy-Arteaga, J. J. Liou, F. J. García-Sánchez, *Microelectron. Reliab.* **2017**, *69*, 1.
[43] L. Chen, S. Li, X. Feng, L. Wang, X. Huang, B. C. K. Tee, K.-W. Ang, *Adv. Electron. Mater.* **2018**, *4*, 1800274.
[44] X. Feng, X. Huang, L. Chen, W. C. Tan, L. Wang, K.-W. Ang, *Adv. Funct. Mater.* **2018**, *28*, 1801524.
[45] Z. Dai, L. Liu, Z. Zhang, *Adv. Mater.* **2019**, *31*, 1805417.
[46] S. Deng, A. V. Sumant, V. Berry, *Nano Today* **2018**, *22*, 14.
[47] T. Liu, S. Liu, K. H. Tu, H. Schmidt, L. Chu, D. Xiang, J. Martin, G. Eda, C. A. Ross, S. Garaj, *Nat. Nanotechnol.* **2019**, *14*, 223.
[48] Z. Li, Y. Lv, L. Ren, J. Li, L. Kong, Y. Zeng, Q. Tao, R. Wu, H. Ma, B. Zhao, D. Wang, W. Dang, K. Chen, L. Liao, X. Duan, X. Duan, Y. Liu, *Nat. Commun.* **2020**, *11*, 1151.
[49] K. Choudhary, G. Cheon, E. Reed, F. Tavazza, *Phys. Rev. B* **2018**, *98*, 014107.
[50] L. Chen, Z. G. Yu, D. Liang, S. Li, W. C. Tan, Y. W. Zhang, K.-W. Ang, *Nano Energy* **2020**, *76*, 105020.
[51] S. Li, B. Li, X. Feng, L. Chen, Y. Li, L. Huang, X. Fong, K.-W. Ang, *npj 2D Mater. Appl.* **2021**, *5*, 1.
[52] B. Tang, Z. G. Yu, L. Huang, J. Chai, S. L. Wong, J. Deng, W. Yang, H. Gong, S. Wang, K.-W. Ang, Y. W. Zhang, D. Chi, *ACS Nano* **2018**, *12*, 2506.

 © 2021 The Authors. Advanced Functional Materials published by Wiley-VCH GmbH